Advances in Sustainable Energies & Environment

Journal homepage: https://A-SEE.MazUST.ac.ir/

Research Article

Design improvement of the Water-rotor Hydrokinetic Turbine to Extract Energy from River Flows and Water Transfer Channels

Sina Chaghamirza, Jafar Nejadali*

Faculty of Engineering and Technology, Department of Mechanical Engineering, University of Mazandaran, Iran

ARTICLE INFO

Article history:
Received: 2025-09-07
Revised: 2025-12-13
Accepted: 2025-12-29
Published: 2026-04-01

Keywords:
Hydrokinetic System;
Numerical Simulation;
Optimization;
Water rotor;
Hub.

ABSTRACT

Hydrokinetic turbines are environmentally friendly systems located in river streams that convert the kinetic energy of water flow into electrical power without the need for a dam. However, due to the low efficiency of these turbines, existing designs are still in the development phase. This study optimizes water-rotor turbine designs—a horizontal-axis, cross-flow variant of Savonius turbines—by simulating six configurations varying blade count (2 or 3) and hub diameter (200-400 mm) at Re=450,000 using ANSYS Fluent with transient k-ω SST turbulence modeling and mesh motion. Three-dimensional finite volume simulations reveal that two-blade designs achieve higher peak power coefficients (Cp-max=0.138 at TSR=0.8 for 200 mm hub) than three-blade ones (Cp-max=0.114 at TSR=0.6), with smaller hubs enhancing performance by maximizing blade cup area. Segmenting the turbine and rotating the rear half by 90° further boosts efficiency to 14.5% at TSR=0.8, outperforming the baseline by 5%. Flow analysis shows reduced wake turbulence and prolonged fluid-blade interaction as key mechanisms, with velocity recovery over 4D downstream informing array spacing. These findings advance dam-free hydropower for rivers and channels.

1. Introduction

With the advancement of technology and the growing global demand for energy, replacing renewable energy sources with fossil fuels—known for their environmental pollution and resource limitations—has become a necessity. Renewable energy sources such as wind, solar, hydro, and geothermal play a significant role in global electricity generation due to their renewability and lack of harmful pollutant emissions [1]. Countries like Norway, Brazil, and New Zealand are pioneers in utilizing these resources, whereas Iran, with a 3.6% share of renewable energy, is still developing this sector [2]. Among renewable energy technologies, hydropower generated through dams is a conventional method [3]. However, hydrokinetic technologies, which utilize natural water flows without requiring dams, have gained attention due to their lower costs and higher sustainability, especially in river and tidal flows [4,5]. These technologies, with high predictability, offer the potential for stable and cost-effective energy production. Iran, with regions such as Qeshm Island, Chabahar Port, and Khuzestan, has significant potential for harnessing this type of energy and can leverage it to reduce dependency on fossil fuels [6].

Khan et al. [7] provided a comprehensive overview of kinetic water energy turbines, classifying them into horizontal-axis and vertical-axis turbines. The primary focus of this study was on hydrokinetic energy conversion systems, which utilize natural flows such as rivers and tidal flows. The findings indicated that, despite advancements in both horizontal and vertical turbines, systems based on channel utilization were given higher priority. This research also explored technologies related to river and tidal flows, with particular attention to the early developments in this field.

Golecha et al. [8] investigated the effect of a deflector plate on the performance of a Savonius turbine. Various configurations for positioning the plate were simulated. The

* **Corresponding author:**
E-mail address: *J.nejad@umz.ac.ir*

Cite this article as:
Chaghamirza, S., & Nejadali, J. (2026). Design improvement of the Water-rotor Hydrokinetic Turbine to Extract Energy from River Flows and Water Transfer Channels. *Advances in Sustainable Energies & Environment* 1 (2) 8 - 18. https://doi.org/10.22034/a-see.2025.2071106.1010

results demonstrated that with an optimal plate placement, turbine efficiency could improve significantly, increasing the power coefficient from 14% to 21% and the torque coefficient from 20% to 26%, representing a 50% power output increase.

Rachman et al. [9] analyzed the impact of blade count (2, 3, and 4 blades) on the performance of horizontal-axis turbines. The results indicated that 2 and 3-bladed turbines performed better at higher rotational speeds, while 4-bladed turbines experienced reduced efficiency in such conditions due to a lower angle of attack. Additionally, increasing the blade count enhanced the generated torque at lower rotational speeds.

Ruopp et al. [10] compared numerical simulations with operational results and studied various components of hydrokinetic turbines. They also examined the performance of a turbine installed in the St. Lawrence River since 2010, reporting its successful operation. This installation was highlighted as one of the most successful full-scale comercialized examples and served as a benchmark for other projects.

Mutule and Kalnacs [11] explored the potential of river free-flow systems and the advantages of power generation from river flows compared to tidal flows. They proposed methods such as using diffusers and internal channels to increase water flow speed. Additionally, energy production estimates based on river width and depth were provided, showing that portions of a river cross-section could be used for power generation without interfering with other uses such as transportation or recreation.

Sarma et al. [12] compared Savonius hydrokinetic turbines with Savonius wind turbines. Their experiments revealed that as flow velocity increased, torque and generated force also rose, but the turbine lifespan decreased. They concluded that hydrokinetic turbines had higher efficiency than wind turbines under similar conditions.

Shahsavarifard et al. [13] studied the effect of casing and diffuser on the performance of horizontal-axis hydrokinetic turbines. Their research showed that using a diffuser could significantly increase the turbine's power coefficient, particularly at flow speeds below 0.9 m/s.

Jenne et al. [14] analyzed the cost of energy production for six flow energy conversion devices, three of which were hydrokinetic turbines (RM1 for tidal flows, RM2 for river flows, and RM3 for ocean flows). The RM3 system demonstrated the best performance in terms of capacity factor (0.7) and energy cost, while the RM1 and RM2 systems had capacity factors of 0.3.

Hauck et al. [15] studied the preliminary design of the "Achard" turbine, which features three straight blades on a vertical axis. Four of these turbines were arranged sequentially on a single shaft with a 90-degree rotation between each. The study compared the Achard turbine with the Darrieus and Gorlov turbines. Results showed that the Achard turbine, with an efficiency of 33%, outperformed the Darrieus (31%) and Gorlov (26%) turbines in a water flow with a velocity of 2.3 m/s.

The objective of this research is to examine the design of a turbine type called the "Water Rotor," focusing on improving its overall efficiency by analyzing various blade configurations for two-blade and three-blade designs. This turbine has a structure similar to the Savonius turbine, with the key difference being that the Savonius turbine is a vertical-axis turbine whose blades partially overlap. In contrast, the Water Rotor is a horizontal-axis turbine with its rotating axis positioned perpendicular to the water flow direction, hence referred to as a cross-flow turbine. The Water Rotor's blades have a plate-like shape similar to the Savonius turbine, but with a hub at the center of the blade section, preventing blade overlap. The performance of this turbine is evaluated through the design of its sections using SolidWorks software and simulations conducted in ANSYS Fluent.

2. Equation

The mechanical power extracted by the turbine is calculated using Equation 1:

$$P = \frac{1}{2}\rho A V^3 \quad (1)$$

Where P: Power output (W), ρ: Fluid density (kg/m³), A: Projected area of the turbine perpendicular to the flow (m²) and V: Fluid velocity (m/s) [16].

Reynolds Number:

$$Re = \frac{\rho U D}{\mu} \quad (2)$$

Where Re: Reynolds Number, U: Free-stream water velocity (m/s), D: Rotor diameter (m), and μ: Dynamic viscosity of the fluid.

The torque (T) generated by the turbine can be determined using the flow forces acting on the turbine blades. The integral of the forces over the blade surface relative to the radius from the axis of rotation gives the torque:

$$T = \int_{blade\ surface} (r \times F)\, dA \quad (3)$$

Where T: Torque (Nm), r: Position vector from the axis of rotation to the point of force application (m), dA: Elemental area of the blade surface (m^2), F: Force vector acting on dA (N) and the cross is used for calculating only the component perpendicular to r.

The dimensionless torque coefficient (C_m) is calculated as:

$$C_m = \frac{T}{\frac{1}{2}\rho A U^2 R} = \frac{4T}{\rho H D^2 U^2} \quad (4)$$

Where, H is height of the turbine (m).

Power coefficient of the turbine (C_p) is calculated as follows:

$$C_P = \frac{P_{Turbine}}{P_{Available}} = \frac{T\omega^*}{\frac{1}{2}\rho A U^3} = C_m * TSR \quad (5)$$

In cases where the turbine torque or angular velocity is not available, the turbine power can be calculated using the second formula [17].

In hydrokinetic turbines, the ratio of the rotor's tangential speed to the flow velocity is defined as the Tip Speed Ratio (TSR), which is a dimensionless parameter used for comparing

different water flow velocities and turbine designs. TSR can be calculated using Equation 6 [8]:

$$\text{TSR} = \frac{\omega D}{2U} \quad (6)$$

In this equation, ω is the angular velocity of the rotor, expressed in radians per second (rad/s).

The angular velocity ω can be calculated using Equation 7 [17]:

$$\omega = \frac{2\pi N}{60} \quad (7)$$

Where N is the rotor speed in revolutions per minute (RPM).

To calculate the time step based on angular velocity, assuming a one-degree rotation per step, Equation 8 is used. For cases requiring multiple degrees of rotation per step, the desired angle must be multiplied in the equation:

$$T_s = \frac{\frac{60}{\omega \times 60}}{\frac{2\pi}{360}} \quad (8)$$

The overall efficiency of the hydrokinetic system is calculated using Equation 9:

$$\eta_t = \eta_m \times \eta_e = \frac{P_m}{P_a} \times \frac{P_e}{P_m} \times 100 = \frac{P_e}{P_a} \times 100 \quad (9)$$

Where η_e: Efficiency of electronic devices (generator, transformer and transmission lines), typically between 85-90%, η_m: Mechanical efficiency of the turbine, P_e: Electrilcal energy output from the generator, P_m: Mechanical energy output from the turbine and P_a: Potential energy in the water flow. The efficiency of river flow turbines is approximately 25%, while ocean current turbines have efficiencies ranging from 35% to 45% [16].

Equation 10 can be used to calculate the deviation percentages:

$$Deviation\ Percentages = \frac{|Cp_{Reference} - Cp_{Simulation}|}{Cp_{Reference}} \times 100 \quad (10)$$

3. Turbine Design

The design of the Water Rotor turbine utilizes the diameter and height specifications from the study by Jaohindy et al. [19]. The turbine has a diameter of 0.904 meters and a height of 1 meter. To achieve maximum mechanical efficiency, six different Configuration for the Water Rotor turbine have been considered, with their specifications detailed in Table 1 and illustrated in Fig.1.

In Fig.2, the schematic of the turbine cross-section is presented. In this figure, a represents the hub diameter, and b denotes the cup diameter of the turbine blades. These values are identical for both the two-blade and three-blade cross-sections.

To enhance accuracy and bring the design closer to real-world construction, two circular plates with a thickness of 2 mm are placed at the front and rear of the turbine. These plates are used to separate the fluid flow around the turbine from the flow that directly interacts with the blades, which can improve the turbine's output efficiency. These two plates are utilized for all six sections, and an example is shown in Fig.3.

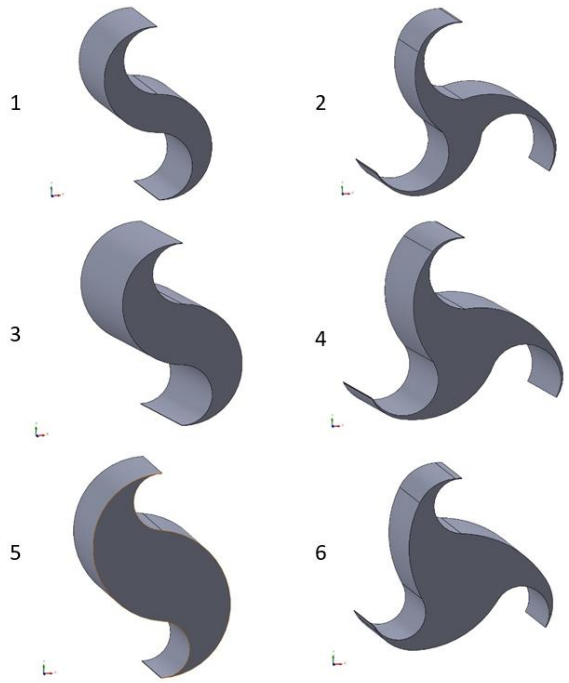

Fig.1. Illustration of designed configuration based on the specifications in table 1

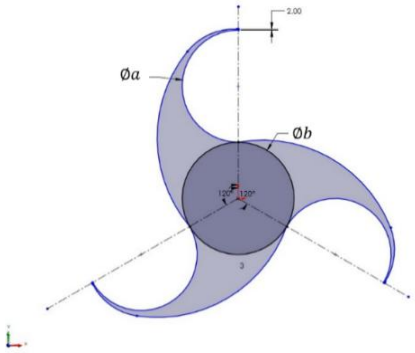

Fig.2. Schematic of the turbine cross-section

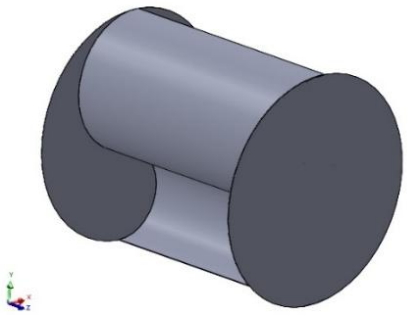

Fig.3. The first configuration of turbine with two front and rear circular plates

Table 1. Specifications of the designed configuration

Section	a (mm)	Number of Blades	b (mm)
1	200	2	350
2	200	3	350
3	300	2	400
4	300	3	400
5	400	2	450
6	400	3	450

4. Numerical Simulation

For simulating the turbine as a rotating region in Ansys Fluent software, as showing in the Fig.4, a control volume with a diameter of 2 meters and a height of 1.4 meters is considered, with a distance of 0.2 meters from the front and rear of the turbine. Within this control volume, the internal volume of the turbine is removed, and the turbine appears as a wall inside the control volume. This approach allows the torque exerted on the wall, which represents the turbine blade surfaces, to be calculated during the simulation.

Far Field is designed as an elongated rectangle to effectively capture the flow conditions downstream of the turbine. A cutout matching the dimensions of the rotating section is made within this area, allowing for seamless integration of the flow from the rotating section into the Far Field. The layout of this area is shown in Fig.5. The computational domain includes two distinct regions—rotational and far-field—each requiring tailored meshing. For the rotational zone, where the turbine is represented as a wall, finer and more precise meshing is essential since this is where primary torque calculations are conducted.

Conversely, the far-field region, acting as a computational space for fluid entry and exit, can utilize coarser meshing to reduce simulation time and computational costs.

The mesh size in the rotational zone is set to 0.03 meters, with the total number of mesh elements varying between 1,390,000 and 1,450,000 depending on the turbine configuration. As shown in the Fig.6, To ensure higher accuracy near the walls, 7 boundary layers are implemented with a growth rate of 1.3. For the rotating region, the mesh exhibited an average aspect ratio of approximately 2.5 with a maximum aspect ratio up to about 100, indicating a small number of highly stretched elements near the rotating parts; the average skewness was about 0.21 with a maximum below 1.0, and the minimum orthogonal quality was roughly 0.005 with an average around 0.78.

The far-field region can be meshed once and reused for all six turbine configurations, as only the rotational zone varies with different turbine designs while the far-field geometry remains unchanged. Automatic meshing is applied to this region with a mesh size of 0.5 meters, resulting in a total of 705,061 mesh elements. Fig.7 Shows the meshing of the Far Field. In this region, had an average aspect ratio of about 1.8 and a maximum of about 9.5, an average skewness of about 0.22 with a maximum below 0.83, and a minimum orthogonal quality of about 0.17 with an average around 0.77.” The computational domain is divided into two regions: the rotational zone and the far-field zone.

The rotational zone, which encompasses the turbine blades, is configured in the software to enable mesh motion. The far-field zone remains stationary, and the interaction between these two regions is established using the “Interface” command. Mesh independence refers to the consistency of simulation results regardless of changes in mesh size or element count. Mesh independence was examined to ensure that the simulation outcomes are not influenced by mesh size.

Various mesh sizes were selected for the rotational and far-field zones, and the turbine along with its surrounding regions was meshed using these different sizes. Simulations were conducted separately for each mesh size, and the results were recorded. The simulation results, including torque coefficient, fluid pressure, and velocity, were compared across different mesh sizes. It was observed that reducing the mesh size improved simulation accuracy. However, after reaching a certain mesh size, further reduction had negligible impact on the results. For the rotational zone, a mesh size of 0.03 meters was determined to be optimal, while for the far-field zone, a mesh size of 0.5 meters was selected. These sizes were chosen to balance accuracy and computational time effectively. A comparison of these mesh sizes is illustrated in Fig. 8.

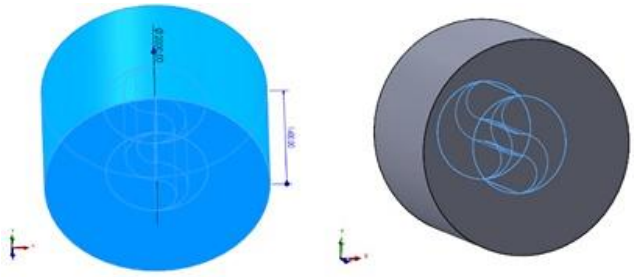

Fig.4. Turbine control volume, rotating region of simulation

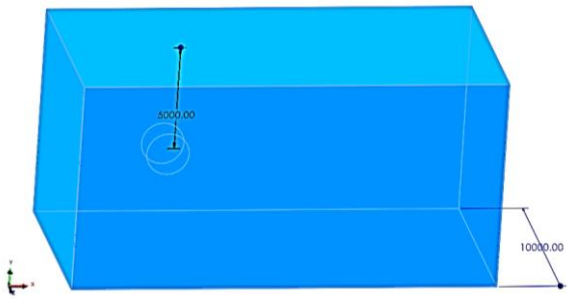

Fig.5. Far Field Area with Dimensions 10×10×20

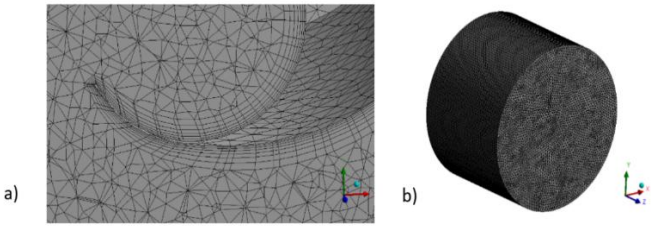

Fig.6. Computational grid

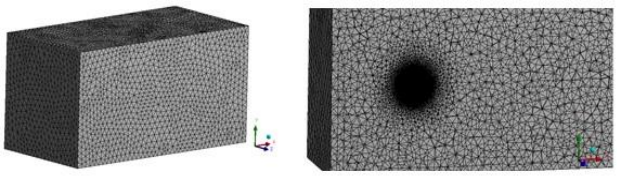

Fig.7. Far Field Mesh

As illustrated in Fig. 8, the differences in power coefficient between the three finest mesh sizes (0.04, 0.03, and 0.02 m) are small, with about a 4% change between 0.04 and 0.03 m and roughly 2.5% between 0.03 and 0.02 m. Consequently, a mesh size of 0.03 m is selected for the simulations as it provides a good compromise between numerical accuracy and computational cost, while ensuring mesh-independent results.

The simulations were conducted using ANSYS Fluent 18.2 in transient mode with the k-ω SST turbulence model, employing the SIMPLE algorithm and second-order discretization for the momentum, turbulent kinetic energy, and specific dissipation rate equations. The numerical solution used carefully selected solution controls to ensure stability and convergence, with under-relaxation factors of 0.3 for pressure, 0.8 for density, 0.8 for body forces, 0.45 for momentum, 0.55 for turbulent kinetic energy, 0.55 for specific dissipation rate, and 0.7 for turbulent viscosity. Convergence was monitored using the residuals of continuity, the three velocity components, turbulent kinetic energy, and specific dissipation rate, with an absolute residual criterion of 1×10^{-3} imposed for all equations. Water, with a river density of 1024 kg/m³ and a viscosity of 0.001003 $kg\cdot m^{-1}\cdot s^{-1}$, was chosen as the fluid. The Reynolds number of the flow interacting with the turbine is 450,000. Using Eq. 2, the inlet flow velocity was calculated as 0.485 m/s. All turbine sections operate under this flow velocity. The outlet boundary condition was set to zero relative pressure. To determine the turbine's maximum power, angular velocities corresponding to TSR values in the range of 0.5 to 1.1 were simulated.

The total simulation time accounted for four complete rotations of the turbine, with each time step corresponding to a 1° rotation.

Time independence in this study is evaluated by varying the time step and the total simulation duration. The time step is defined based on the time required for the turbine to rotate by one degree, and it is therefore directly related to the angular velocity of the rotor. Consequently, for each specific angular speed, a corresponding and consistent time step is selected. Since the simulations are conducted over a range of 0.5 to 1.4 TSR, the rotational speed of the turbine changes throughout this range, leading to variations in the time step as well. Although the time-step value in seconds is not constant during the simulations, its ratio to a one-degree rotation of the turbine remains fixed to ensure that the dynamic behavior of the flow is accurately captured.

To assess time independence, the turbine's output power is calculated for various time-step sizes corresponding to angular rotations of 0.5°, 1°, 1.5°, and 2°. The resulting values are then compared. If the differences between these results are negligible, the simulation can be considered time-independent.

For this evaluation, a tip speed ratio (TSR) of 1 is considered, and the time steps corresponding to the above angular increments are calculated using Eq. (8) in Table 2. The simulation results for each time step are presented in Fig. 9.

As illustrated in Fig. 9, the differences in power coefficient between the three lowest time step (0.00812, 0.01624, and 0.02436 s) are small, with about a 5% change between 0.02436 and 0.01624 s and roughly 1% between 0.01624 and 0.00812 s. Consequently, a time step of 0.01624 s that is representative as 1 degree rotation is selected for the simulations as it provides a good compromise between numerical accuracy and computational cost, while ensuring time step independent results. The total simulation time is selected to cover four complete revolutions of the turbine.

The final torque value is obtained by averaging the torque over the last revolution, as the flow typically requires several initial revolutions to reach a quasi-steady state and the early results may not be reliable. Therefore, to confirm time independence, the torque and power values obtained from multiple revolutions are examined to identify which revolution yields stable and accurate results. Given that each time step represents one degree of rotation, if the simulation progresses for 1,440-time steps, the turbine completes four full revolutions. To examine overall time independence, the simulation is extended to five revolutions, corresponding to 1,800-time steps. The resulting torque values obtained over these five revolutions are then analyzed under the same conditions used previously for the time step-independence assessment.

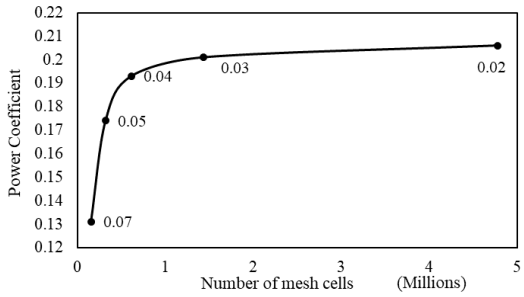

Fig.8. Mesh independence analysis for Savonius Turbine and TSR=1, Relative to Fig. 13 results

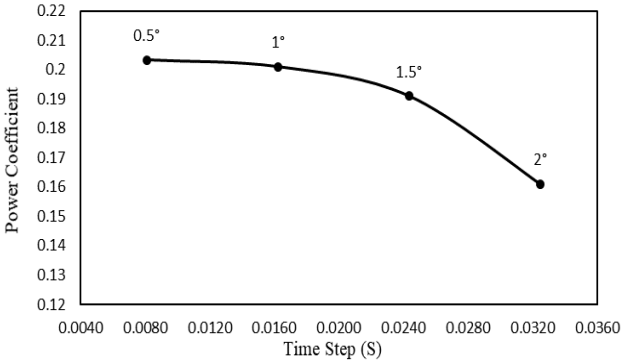

Fig.9. Time independence analysis for Savonius Turbine and TSR=1, Relative to Fig. 13 results

Table 2. Time step based on degree of rotation

Degree	Time step (s)
0.5	0.00812
1	0.01624
1.5	0.02436
2	0.03248

The numerical results obtained are presented in Table 3. As shown in Table 3, the value obtained for the first revolution deviates significantly, exhibiting a difference of more than 50%. However, the values corresponding to revolutions 2, 3, 4, and 5 differ by only about 2–3%. Therefore, to ensure sufficiently accurate and reliable results, the data obtained from the fourth revolution are used in subsequent analyses.

5. Validation

For validation purposes, the turbine presented in Jaohindy et al.'s study was re-simulated using the methods described in this research. The results of this simulation, conducted in water as the working fluid, are compared with the results obtained using air as the working fluid in the referenced study. Additionally, an earlier experimental study by Sheldahl et al. [18], which was cited in the reference article, was utilized for validation. The results from both studies are used to verify this research. The dimensions and geometry of the Savonius turbine, depicted in Fig.10, are identical to those of the Water Rotor turbines, with the main difference being the cross-section and blade design [19].

The rotating and far-field regions of this turbine are similar to the previous design. For meshing, a mesh size of 0.03 was used, resulting in a total of 1,436,605 mesh elements within the rotating region. After simulating the turbine and obtaining the results, the torque coefficient chart for four turbine rotations at a TSR of 0.9 is illustrated in Fig. 11. According to this chart, a periodic cycle of the torque coefficient exists for this turbine. To determine an overall efficiency for the turbine, the torque coefficient for a single turbine rotation is averaged. The resulting average value represents the torque coefficient for this turbine's cross-section. The torque coefficient values obtained for the turbine were averaged over the final rotation, and the results were calculated for TSR values between 0.5 and 1.4. Using the torque coefficient, the turbine's power coefficient can be determined through Eq. 5. Based on Fig. 12 and Fig. 13, it is observed that the results obtained from this simulation align well with the findings of the two previous studies. This confirms the reliability of the simulation method employed.

The power coefficient obtained from the present simulation was validated against two experimental datasets extracted from Jaohindy et al.'s study. The deviation percentages between the numerical and experimental values was computed with Eq. 10 for each TSR. The corresponding values are summarized in Table 4.

Table 3. Power coefficient value over number of revolutions

Revolution	Cp
1	0.3181
2	0.2038
3	0.1982
4	0.2018
5	0.2058

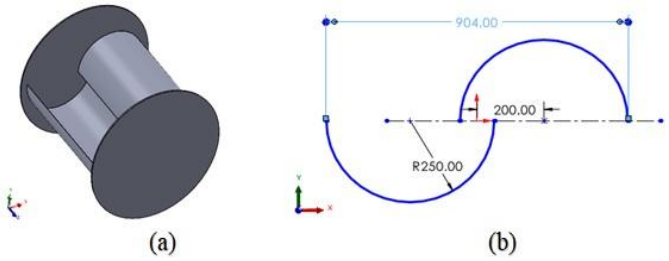

Fig.10. a) Designed turbine and b) Cross-Section of the Savonius Turbine

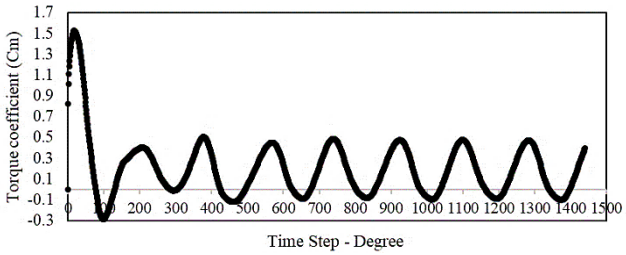

Fig.11. Torque coefficient values over 4 turbine rotations equivalent to 1440 Time Steps

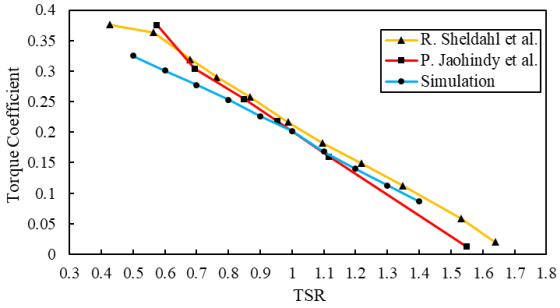

Fig.12. The Torque coefficient in terms of TSR

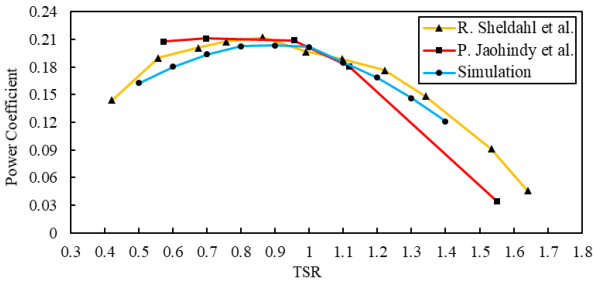

Fig.13. The Power coefficient in terms of TSR

Table 4. Comparison of numerical deviation percentages

TSR	Cp (simulation)	Cp (R. Sheldahl et al.)	Cp (P. Jaohindy et al.)	Deviation from (R. Sheldahl et al.)	Deviation from (P. Jaohindy et al.)
0.6	0.1804	0.1942	0.2084	7.11%	13.44%
0.7	0.1939	0.2034	0.2107	4.67%	7.97%
0.8	0.2024	0.2093	0.2093	3.30%	3.30%
0.9	0.2033	0.2089	0.2089	2.68%	2.68%
1	0.2018	0.1961	0.2016	2.91%	0.10%
1.1	0.185	0.1892	0.1819	2.22%	1.70%
1.2	0.1683	0.1792	0.1531	6.08%	9.93%
1.3	0.1464	0.1581	0.1197	7.40%	22.31%
1.4	0.1208	0.1316	0.0859	8.21%	40.63%

As shown in Table 2, the simulation exhibits very good agreement with both experimental studies over most of the operating range, particularly between TSR = 0.6 and 1.3, where the deviation with respect to the first dataset remains below about 8%, and for TSR = 0.7–1.2 even below about 5%. The differences with the second dataset are generally within 2–9% up to TSR = 1.2, indicating that the numerical model is able to reproduce the peak and the descending part of the power coefficient curve with acceptable accuracy.

Larger deviations are observed at higher TSR values, where the percentages increase to approximately 8–9% for the first dataset and up to about 40% for the second dataset at TSR = 1.4. This behavior is consistent with the increased sensitivity of the turbine performance to stall, three dimensional effects and measurement uncertainty in this high TSR region. Overall, the comparison confirms that the present CFD model provides reliable predictions of the turbine power coefficient in the main operating range, and the remaining discrepancies at high TSR can be attributed to the limitations of both the experiments and the numerical assumptions.

6. Results and discussions

As demonstrated in the validation section for the Savonius turbine, the performance of this type of water rotor turbine resembles that of Savonius turbines, characterized by periodic force behavior. Increasing the number of blades results in a corresponding increase in periodicity. As illustrated in Fig. 14 and Fig. 15, the 2-blade Configuration exhibits 2 periodic cycles, while the 3-blade Configuration exhibits 3 periodic cycles during one full turbine rotation. Therefore, adding more blades leads to higher periodicity in turbine performance.

To calculate the turbine power efficiency percentage, the simulation results obtained for each degree of turbine rotation are averaged over a complete rotation. This average is then multiplied by the TSR value at which the simulation was conducted to determine the turbine's power efficiency percentage. The calculated values for each Configuration and for TSRs ranging between 0.5 to1.1 are tabulated in Table 5. Based on Table 5, the highest efficiency occurs in Configuration 1, which corresponds to the 2-blade turbine with a 200 mm hub, while the lowest efficiency is observed in Configuration 6, featuring a 3-blade turbine with a 400 mm hub. This ranking highlights a fundamental design trade-off: while more blades increase torque frequency, they also amplify fluid dynamic interference between adjacent blades, which can degrade net performance.

Fig. 16 and Fig. 17 illustrate the power coefficient and torque performance for the 3-blade turbine Configuration. As shown, increasing the hub size leads to a decrease in turbine efficiency. One primary reason for this decline is the reduction in the turbine blade cup area. This reduction diminishes the effective swept area for energy capture, directly lowering the potential torque according to the fundamental relationship between force, pressure, and surface area. For TSR values greater than 1.1, their efficiency turns negative, meaning they no longer generate power effectively at these rotational speeds. The peak efficiency for these turbines occurs at a TSR of 0.6.

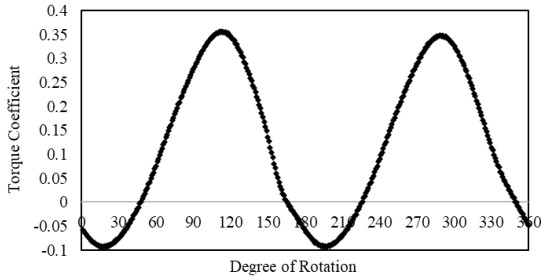

Fig.14. Number of periodic cycles for the 2-Blade turbine in one complete rotation

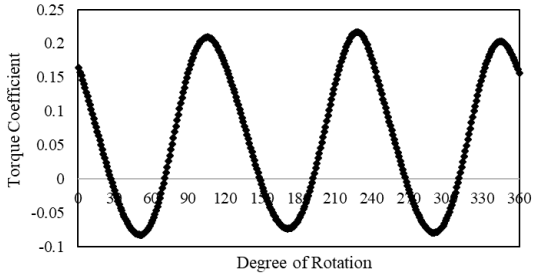

Fig.15. Number of periodic cycles for the 3-blade turbine in One Full Rotation

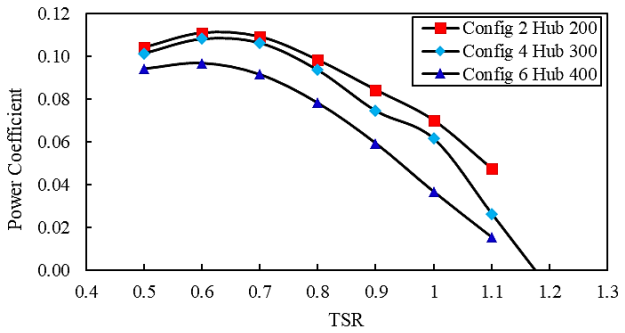

Fig.16. Power coefficient performance of three-blade turbine configuration

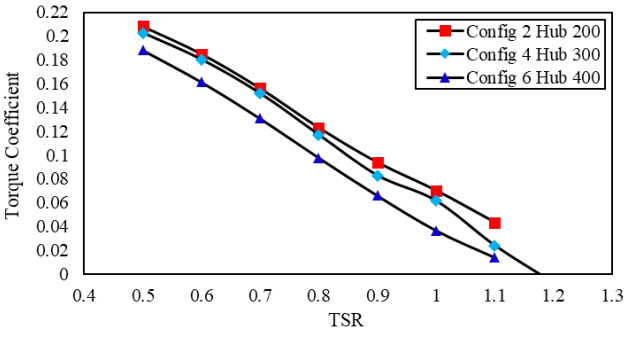

Fig.17. Torque performance of three-blade turbine configuration

Table 5. Output power efficiency percentage of six water turbine rotor configurations

TSR	Configuration					
	1	2	3	4	5	6
0.5	11.1	10.4	9.4	10.1	7.9	9.4
0.6	12.7	11.1	11.1	10.8	9.3	9.7
0.7	13.6	10.9	11.5	10.6	9.7	9.1
0.8	13.8	9.8	11.4	9.4	9.4	7.8
0.9	12.5	8.4	10.4	7.4	8	5.9
1	10.3	7	8.1	6.1	5.8	3.6
1.1	6.6	4.7	5.2	2.6	3	1.5

To analyze the fluid flow around the turbine configuration, pressure and velocity contours, along with velocity vectors near the turbine, are examined. As illustrated in Fig.18 ,19 and 20, during the simulation at a specific time step, a high-pressure zone develops at the front of the turbine due to the direct impact of the incoming fluid on the blade facing the flow. This interaction redirects the fluid upwards and downwards, resulting in the formation of a low-pressure zone behind the turbine. The turbine body functions similarly to a spoiler, accelerating the fluid and channeling it toward the blades. This mechanism enhances the energy transfer from the fluid to the turbine.

According to Fig.20, the velocity vectors illustrate the formation of two distinct vortices corresponding to the turbine blades positioned upstream and downstream relative to the flow. The upstream blade generates a vortex as it obstructs the incoming flow, while the downstream blade induces a similar effect due to the flow's separation. Additionally, a low-velocity wake region is evident behind the turbine, resulting from drag forces. This wake zone contains secondary vortices that form and dissipate dynamically as the turbine rotates, highlighting the complex interaction between the blades and the surrounding fluid. Two-bladed turbines exhibit distinct differences in performance compared to their three-bladed counterparts, particularly in the location of their peak efficiency. For two-bladed designs, the peak efficiency is achieved at higher TSR values, indicating a shift in optimal operational conditions. Furthermore, the effect of hub size is more pronounced in two-bladed turbines, resulting in a more significant disparity in efficiency between configurations. As depicted in Figs. 21 and 22, the first configuration, featuring a 200 mm hub, outperforms the others, achieving a maximum efficiency of 13.8% at a TSR of 0.8. This highlights the critical role of hub size in optimizing turbine performance.

The fluid behavior around the two-bladed turbine closely resembles that of the three-bladed turbine. However, in the two-bladed design, the interaction time between the fluid and the turbine cup is longer, allowing it to extract more energy from the fluid compared to the three-bladed turbine. Increased turbulence and flow disturbance in the wake region reduce the efficiency of both turbine types; however, the turbulence intensity is lower for the two-bladed configuration.

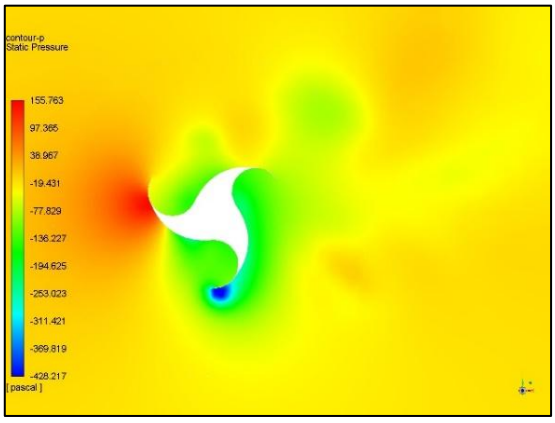

Fig.18. Pressure contour for configuration 4 with a 300mm hub

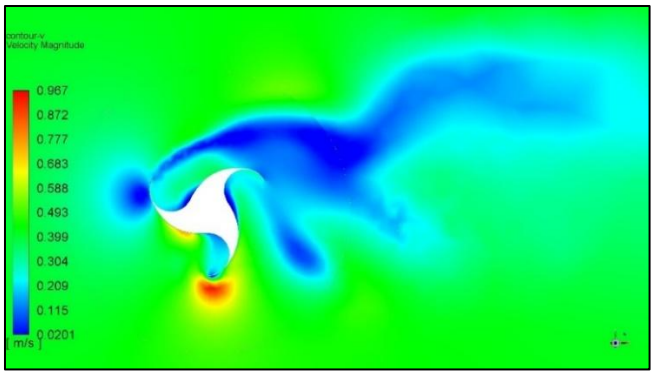

Fig.19. Velocity contour for configuration 4 with a 300mm hub

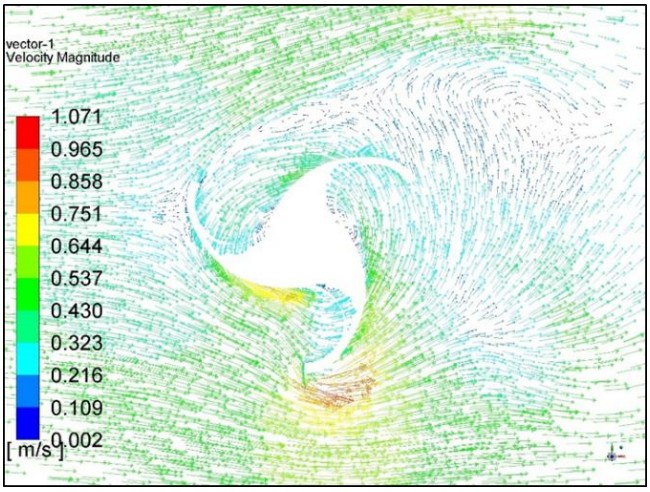

Fig.20. Velocity vectors for configuration 4 with a 300mm hub

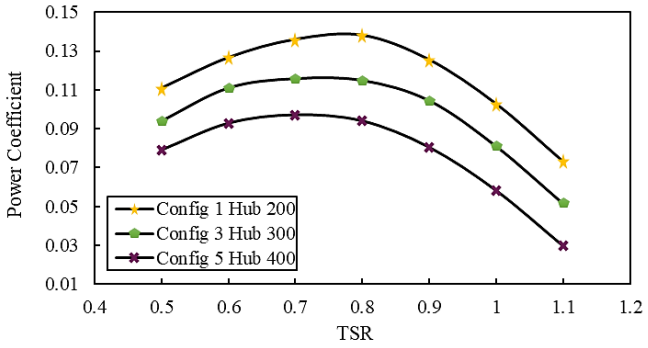

Fig.21. Power coefficient of two-blade turbine configuration

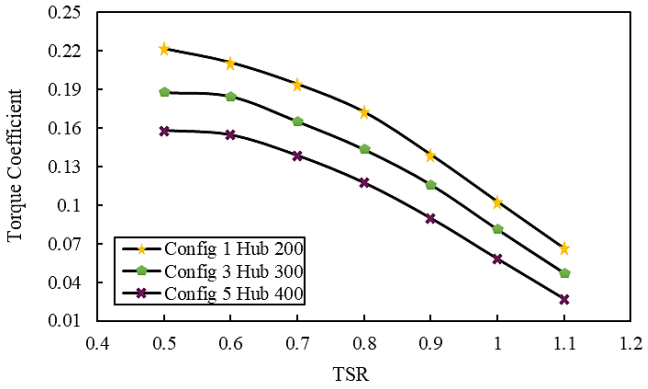

Fig.22. Torque coefficient of Two-Blade Turbine Configuration

Additionally, the sudden localized pressure drop observed at the turbine's edge at a specific time step, increases the likelihood of cavitation. Nonetheless, cavitation requires a significant pressure drop, and as shown in the pressure contour in Fig.23, the observed pressure reduction is not substantial enough to cause water to transition into a two-phase flow or initiate cavitation. By examining the velocity contours for the 2-blade and 3-blade Configuration, shown in Fig.24 and Fig.19, it can be concluded that the turbulence and velocity reduction occurring behind the turbine take approximately four times the turbine diameter to dissipate and return to normal flow conditions. Considering this, if the turbines are to be arranged in an array or placed in sequence, a spacing of about four times the turbine diameter should be maintained to minimize the impact of one turbine on the flow entering the next. In this section, a single vortex forms behind the turbine blade, whereas in the three-blade turbine, vortices were generated behind both blades that were not in direct contact with the flow. The formation of vortices and the distance required for the flow behind the turbine to regain its initial velocity and condition can significantly impact the turbine performance. The velocity vector of the fluid is depicted in Fig. 25.

The comprehensive analysis of the simulation results, illustrated in Fig. 26 reveals that, in general, three-blade configurations with identical dimensions exhibit lower efficiency compared to two-blade configurations. Additionally, as the hub size decreases and the blade cup size increases, the turbine is able to capture more energy from the fluid, thereby achieving higher efficiency. The first configuration of the turbine demonstrates the highest efficiency across its entire rotational speed range. To enhance the turbine performance and increase efficiency, simulations were conducted at a TSR of 0.8, incorporating varying rotations of the turbine's second half based on the segmented design concept. the cylindrical length of the turbine is divided into two segments. The second segment is rotated and positioned at a different angle relative to the first segment. To determine the angle that maximizes efficiency, four configurations with angles of 20 degrees, 40 degrees, 60 degrees, and 90 degrees are evaluated. A 90-degree example of this design, applied to the first section that has two blades and a 200-mm hub, is illustrated in Fig. 27.

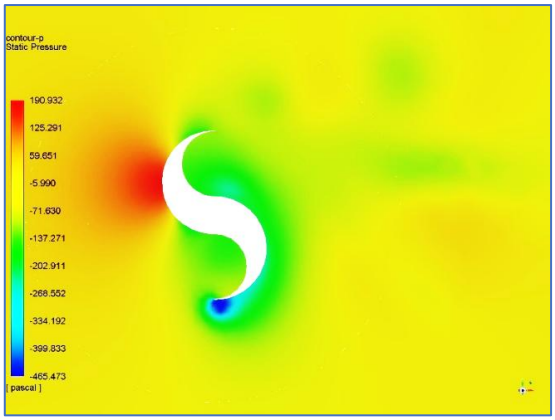

Fig.23. Pressure contour for the first configuration with a 200 mm hub

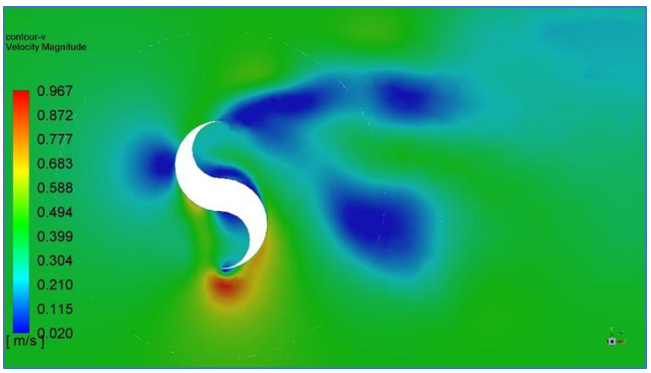

Fig.24. Velocity contour for the first Configuration with a 200 mm Hub

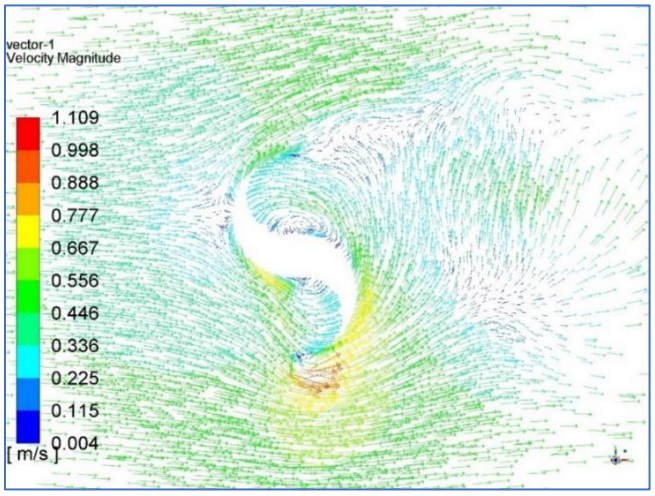

Fig.25. Velocity vectors for the two-blade turbine in the first Configuration with a 200 mm hub

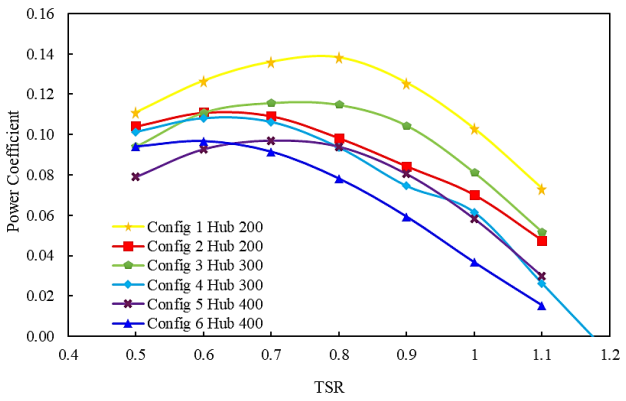

Fig.26. Comprehensive performance of water-rotor turbine configurations

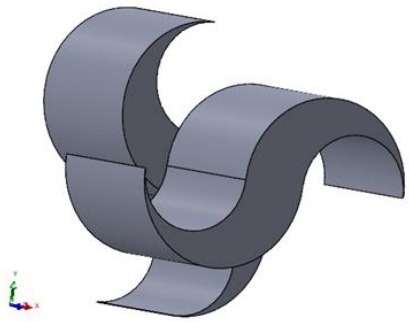

Fig.27. 90-degree rotation design compared to the original position

These simulations, as illustrated in Fig. 28, revealed that a 20-degree rotation of the second half reduced the turbine's efficiency compared to the unaltered configuration. This decrease is attributed to the disruption of flow patterns caused by the rotation and the presence of the separating plane between the two halves. However, as the rotation angle increases, the turbine's performance improves, ultimately achieving its peak efficiency of 14.5% at a 90-degree rotation.

7. Conclusion

Effective design strategies for enhancing the performance of water-rotor turbines for extracting energy from river flows and water transfer channels, were outlined in this paper. Therefore, numerical simulation of fluid flow using computational fluid dynamics was applied. The key findings include:

• The study demonstrated that two-bladed turbines consistently outperform three-bladed designs in terms of efficiency. The peak power output for two-bladed turbines occurs at a Tip Speed Ratio (TSR) of 0.8, while for three-bladed turbines, it peaks at a TSR of 0.6. This indicates a shift in optimal operational conditions based on blade count.

• Increasing the hub size negatively affects turbine efficiency. The optimal configuration, featuring a 200 mm hub diameter in a two-blade design, achieved a maximum efficiency of approximately 14.5%. This highlights the critical role of hub design in maximizing energy extraction from flowing water.

• The simulations revealed complex fluid dynamics around the turbine, with distinct pressure and velocity contours indicating efficient energy transfer mechanisms. The presence of vortices and wake regions underscores the importance of blade design and spacing for optimizing performance.

• Implementing a segmented design with adjustable angles for the turbine's second half showed potential for further enhancing efficiency. The optimal angle for this configuration was found to be 90 degrees, resulting in improved performance metrics.

• Despite the relatively low energy output of 7.65 W at a water velocity of 0.485 m/s, the study emphasizes the potential for significantly higher energy extraction in faster-moving waters, such as tidal channels, where water velocities exceed 1 m/s.

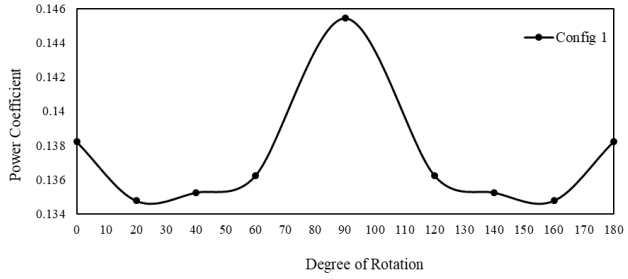

Fig.28. Segmented two-blades turbine with a 200 mm hub at TSR 0.8, considering the second-half rotation

Nomenclature

A	Projected Area in the Flow Direction
C_P	Turbine Power Coefficient
C_m	Turbine Torque Coefficient
dA	Integral Element on blade surface (m²)
D	Rotor Diameter (m)
F	Force Vector Acting on Element dA (N)
H	Turbine Height (m)
N	Rounds Per Minute (RPM)
P	Turbine Mechanical Power (W)
P_0	Actual annual turbine production capacity (W)
p	Fluid Pressure (Pa)
r	Position Vector from the Axis of Rotation (m)
Re	Reynolds Number
R	Rotor Radius (m)
T	Torque (N·m)
TSR	Tip Speed Ratio
U	Free Flow Velocity (m/s)
V	Fluid Flow Speed Rate (m/s)
α	Hub Diameter (m)
β	Cup Diameter (m)
μ	Viscosity (Pa·s)
ω	Angular Velocity (rad/s)

Data availability statements:

The data that support the findings of this study are available from the corresponding author upon reasonable request.

Declarations:

Funding Statement: This research did not receive any specific grant from funding agencies in the public, commercial, or not-for-profit sectors.

Authors' contributions: The authors contributed equally to this article.

Acknowledgements:

Conflict of interest: The authors declare that they have no known competing financial interests or personal relationships that could have influenced the work reported in this paper.

References

[1] M. Liu, Hydrokinetic turbine power converter and controller system design and implementation, Ph.D. Dissertation, University of British Columbia, 2014.

[2] Enerdata, Renewables in electricity production: Statistics map by region. https://yearbook.enerdata.net/renewables/renewable-in-electricity-production-share.html, 2023 (accessed 4 January 2024).

[3] M.S. Güney, K. Kaygusuz, Hydrokinetic energy conversion systems: A technology status review, Renew. Sustain. Energy Rev. 14 (2010) 2996–3004.

[4] P.K. Yadav, A. Kumar, S. Jaiswal, A critical review of technologies for harnessing the power from flowing water using a hydrokinetic turbine to fulfill the energy need, Energy Rep. 9 (2023) 2102–2117.

[5] M.I. Yuce, A. Muratoglu, Hydrokinetic energy conversion systems: A technology status review, Renew. Sustain. Energy Rev. 43 (2015) 72–82.

[6] S.P. Zanous, R. Shafaghat, R. Alamian, M.S. Shadloo, M. Khosravi, Feasibility study of wave energy harvesting along the southern coast and islands of Iran, Renew. Energy 135 (2019) 502–514.

[7] M.J. Khan, G. Bhuyan, M.T. Iqbal, J.E. Quaicoe, Hydrokinetic energy conversion systems and assessment of horizontal and vertical axis turbines for river and tidal applications: A technology status review, Appl. Energy 86 (2009) 1823–1835.

[8] K. Golecha, T.I. Eldho, S.V. Prabhu, Influence of the deflector plate on the performance of modified Savonius water turbine, Appl. Energy 88 (2011) 3207–3217.

[9] A. Rachman, R. Balaka, J. Delly, Y. Gunawan, Simulation on the effect of the blade number on the rotational characteristic of a horizontal axis river current turbine, Int. J. Energy Environ. Eng. 4 (2013) 1–8.

[10] A. Ruopp, A. Ruprecht, S. Riedelbauch, G. Arnaud, I. Hamad, Development of a hydrokinetic river turbine with simulation and operational measurement results in comparison, IOP Conf. Ser.: Earth Environ. Sci. 22 (2014) 062002.

[11] A. Mutule, A. Kalnacs, Hydro energy potential estimation for hydrokinetic power plants, in: Proc. 15th Int. Sci. Conf. on Electric Power Engineering (EPE 2014), 2014, pp. 297–300.

[12] N.K. Sarma, A. Biswas, R.D. Misra, Experimental and computational evaluation of Savonius hydrokinetic turbine for low velocity condition with comparison to Savonius wind turbine at the same input power, Energy Convers. Manag. 83 (2014) 88–98.

[13] M. Shahsavarifard, E.L. Bibeau, V. Chatoorgoon, Effect of shroud on the performance of horizontal axis hydrokinetic turbines, Ocean Eng. 96 (2015) 215–225.

[14] D.S. Jenne, Y.H. Yu, V. Neary, Levelized cost of energy analysis of marine and hydrokinetic reference models, in: Proc. 3rd Marine Energy Technology Symposium (METS 2015), U.S. Department of Energy, Washington, DC, 2015.

[15] M. Hauck, A. Rumeau, A.I. Bratcu, S. Bacha, I. Munteanu, D. Roye, Identification and control of a river-current-turbine generator—Application to a full-scale prototype, IEEE Trans. Sustain. Energy 9 (2018) 1365–1374.

[16] N.R. Maldar, C.Y. Ng, M.S. Patel, E. Oguz, Potential and prospects of hydrokinetic energy in Malaysia: A review, Sustain. Energy Technol. Assess. 52 (2022) 102265.

[17] T.S. Rengma, M.K. Gupta, P.M.V. Subbarao, A novel method of optimizing the Savonius hydrokinetic turbine blades using Bezier curve, Renew. Energy 216 (2023) 119091.

[18] R.E. Sheldahl, B.F. Blackwell, L.V. Feltz, Wind tunnel performance data for two- and three-bucket Savonius rotors, J. Energy 2 (1978) 160–164.

[19] P. Jaohindy, S. McTavish, F. Garde, A. Bastide, An analysis of the transient forces acting on Savonius rotors with different aspect ratios, Renew. Energy 55 (2013) 286–295.